CRYSTAL GROWTH & DESIGN

Article

Cite This: Cryst. Growth Des. 2019, 19, 6274−6282

pubs.acs.org/crystal

Lead−Organic Frameworks Containing Trimesic Acid: Facile Dissolution−Crystallization and Near-White Light Emission

Mesoun A. A. Al-Nubi,[†] Aliyu M. Hamisu,[†] Fendi Y. Wardana,[†] Azhar Ariffin,[†] Hongil Jo,[‡] Kang Min Ok,[‡] and Arief C. Wibowo*[,§]

[†]Department of Chemistry, University of Malaya, Kuala Lumpur, 50603, Malaysia

[‡]Department of Chemistry, Sogang University, Seoul, 04107, South Korea

[§]Department of Chemistry, Airlangga University, Surabaya, East Java 60115, Indonesia

Supporting Information

ABSTRACT: Three new, closely similar Pb-based organic frameworks synthesized using a simple and optimized dissolution−crystallization method with benzene-1,3,5-tricarboxylic acid (H_3BTC) are reported along with their structural characterizations and photoluminescent properties. Compound **1**, $Pb(HBTC)(1,4\text{-dioxane})_{0.5}$, crystallizes in the $C2/c$ space group (a = 17.239(2) Å, b = 7.0225(8) Å, c = 19.911(2) Å, β = 104.735(10)°); compound **2**, $Pb_2(HBTC)_2(H_2O)_5$, crystallizes in the $P\bar{1}$ space group (a = 7.3989(4) Å, b = 8.2196(4) Å, c = 10.1437(5) Å, α = 94.336(4)°, β = 104.943(4)°, γ = 108.270(3)°); and compound **3**, Pb(HBTC)(DMF), crystallizes in the $P2_1/n$ space group (a = 10.5004(3) Å, b = 7.1398(3) Å, c = 17.1285(5) Å, β = 102.160(2)°). All three compounds are built from a slightly different one-dimensional (1D) structure interconnected into three-dimensional metal−organic frameworks by $HBTC^-$ ligands forming different pore sizes, in which the 1D moieties and pore sizes are governed by the solvent used during synthesis. Among the three compounds, compounds **1** and **2** exhibit solid state photoluminescence with **2** showcasing an interesting, near white-light emission, single-component phosphor with CIE coordinates of (0.33, 0.36).

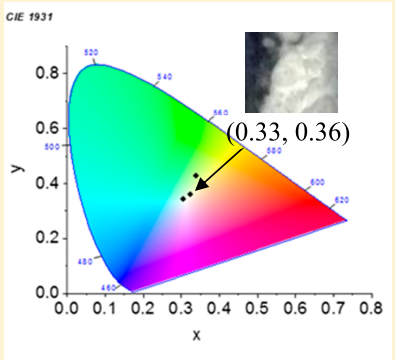

INTRODUCTION

Hydro- and solvothermal synthetic methods are convenient techniques for preparing metal−organic frameworks (MOFs) using aromatic dicarboxylic acid based ligands and transition elements, in particular, post-transition elements, with reported applications such as gas storage,[1−5] magnetic,[1,2,6,7] and luminescent applications.[1,2,8−10] The dissolution−crystallization method, a rather less popular technique and yet requires less synthetic equipment, could potentially produce a new, kinetically stable MOF that may merit its own structural library and applications.[11−41] By a similar token of a facile dissolution−(re)-crystallization technique, postsynthetic modification of MOFs exploits the relatively weak coordination bond of certain metal centers to synthesize new compounds with tunable properties that are not possible through conventional synthetic pathways.[42,43]

Benzene-1,3,5-tricarboxylic acid (H_3BTC) ligand, with or without a coligand, is one of the most frequently used ligands to construct MOFs, including the world-famous HKUST-1, $Cu_3(BTC)_2(H_2O)_3$. To date, HKUST-1 has been reported for catalytic, photocatalytic, enzyme encapsulation, and semiconducting applications.[44−48]

The lead(II) cation, one of the main group cations with lone pair electrons, inherits several advantages, including being tolerant to defects and hence has the possibility of tunable electronic properties; it is one of the borderline acids, thus adaptable to a variety of coordination environments, having variable coordination numbers (2−10) due to its large ionic radii.[49−56] Thus far, there are only five reports about Pb-based BTC, with four disclosed crystal structures.[57−61] Our interest lies in discovering new, lead-based MOFs with exotic properties using a less preferred, but facile, dissolution−crystallization method.

In recent years, there is an immense interest in discovering white-light single phosphors from Pb-based compounds due to its intrinsic broadband emission originated from self-trapping exciton and defects.[62,63] Several white-emitting Pb-based frameworks and coordination polymers (MOCP) have also been reported.[64−66] Enriching the library of single-component, near white-emission Pb frameworks, herein we report three new BTC-containing Pb frameworks, in which compound **2** displays near white-light emission. The compounds are made using a facile dissolution−crystallization method, exploiting the use of the hard−soft acid base (HSAB) principle to find a suitable modulator to yield a phase pure product.

Received: June 13, 2019
Revised: September 29, 2019
Published: October 3, 2019

DOI: 10.1021/acs.cgd.9b00759
Cryst. Growth Des. 2019, 19, 6274−6282

Table 1. Crystal Data and Structure Refinement Details for 1, 2, and 3[a]

	compound 1	compound 2	compound 3
empirical formula	$C_{13}H_{13}O_9Pb$	$C_{18}H_8O_{17}Pb_2$	$C_{12}H_{11}NO_7Pb$
formula weight	520.42	910.62	488.41
temperature (K)	293(2)	203(2)	296(2)
wavelength	0.71073 Å		
crystal system	monoclinic	triclinic	monoclinic
space group	$C2/c$	$P\bar{1}$	$P2_1/n$
unit cell dimensions	a = 17.239(2) Å, α = 90.00°	a = 7.3989(4) Å, α = 94.336(4)°	a = 10.5004(3) Å, α = 90°
	b = 7.0225(8) Å, β = 104.735(10)°	b = 8.2196(4) Å, β = 104.943(4)°	b = 7.1398(3) Å, β = 102.160(2)°
	c = 19.911(2) Å, γ = 90.00°	c = 10.1437(5) Å, γ = 108.270(3)°	c = 17.1285(5) Å, γ = 90°
volume (Å^3)	2331.2(5)	557.70(5)	1255.32(7)
Z	6	1	4
density (calculated) (g/cm^3)	2.224	2.711	2.584
absorption coefficient (mm^{-1})	10.900	15.163	13.476
F(000)	1470	416	912
crystal size (mm^3)	0.12 × 0.032 × 0.024	0.13 × 0.068 × 0.022	0.127 × 0.032 × 0.026
θ range for data collection (°)	2.12−28.26	2.648−28.35	2.433−27.099
index ranges	$-22 \le h \le 21$, $-9 \le k \le 9$, $-25 \le l \le 26$	$-8 \le h \le 9$, $-10 \le k \le 10$, $-13 \le l \le 13$	$-13 \le h \le 13$, $-9 \le k \le 9$, $-21 \le l \le 21$
reflections collected	14566	9327	10151
independent reflections	2857 [R_{int} = 0.0910]	2752 [R_{int} = 0.0683]	2686 [R_{int} = 0.0719]
completeness to θ = 27.56° (%)	98.4	99.5	97.8
refinement method	full-matrix least-squares on F^2		
data/restraints/parameters	2857/0/174	2752/122/169	2686/0/190
goodness-of-fit	1.000	1.006	1.029
final R indices [$I > 2\sigma(I)$]	R_{obs} = 0.0389, wR_{obs} = 0.0737	R_{obs} = 0.0471, wR_{obs} = 0.1125	R_{obs} = 0.0371, wR_{obs} = 0.0683
R indices [all data]	R_{all} = 0.0635, wR_{all} = 0.0819	R_{all} = 0.0616, wR_{all} = 0.1207	R_{all} = 0.0567, wR_{all} = 0.0767
largest diff = peak and hole	1.523 and −1.321 e·Å^{-3}	3.343 and −2.571 e·Å^{-3}	1.384 and −1.087 e·Å^{-3}

[a] $R = \sum ||F_0| - |F_C|| / \sum |F_0|$. $wR_2 = \{\sum [w(F_0^2 - F_C^2)^2] / \sum [w(F_0^2)^2]\}^{1/2}$.

EXPERIMENTAL SECTION

All reagents are commercially available and used without further purification. $Pb(NO_3)_2$ (≥99.0%), benzene-1,3,5-tricarboxylic acid (95.0%), aniline (≥99.5%), and imidazole (≥99.0%) were purchased from Sigma-Aldrich. Solid-state UV−vis and photoluminescent spectra were recorded on UV−vis-NIR Lambda 950, PerkinElmer spectrophotometer and FLS920 Edinburgh instruments, respectively. Attenuated total reflectance Fourier-transform infrared (ATR-FTIR) spectra were recorded on a PerkinElmer FTIR-Spectrum 400. TGA analysis was conducted using PerkinElmer SII Pyris Diamond TG/DTA thermogravimetric/differential thermal analyzers. Elemental analyses were performed using a PerkinElmer CHNS/O 2400 Series II. Electron microscopy images were obtained using a Hitachi SU8220 scanning electron microscope-energy dispersive spectrometry (SEM-EDS).

Synthesis of Pb(HBTC)(1,4-dioxane)$_{0.5}$ (1). $Pb(NO_3)_2$ (0.0331 g, 0.1 mmol) dissolved in 4 mL of distilled water was carefully layered on top of H_3BTC (0.021 g, 0.1 mmol) dissolved in 8 mL of 1,4-dioxane, with careful addition of aniline (0.0272 g, 0.4 mmol). White ribbon-like crystals were formed after ca. 3 days with a nearly quantitative yield. The final products were washed thoroughly with fresh DI water, isolated by vacuum filtration, and dried at room temperature. A quantitative analysis of the crystals obtained was performed by CHN analysis. Anal. calcd (Found) for $C_{13}H_{13}O_9Pb$: C, 29.99 (30.02); H, 2.52 (2.49).

Synthesis of Pb$_2$(HBTC)$_2$(H$_2$O)$_5$(2). $Pb(NO_3)_2$ (0.0331 g, 0.1 mmol) dissolved in 4 mL of distilled water was carefully layered on top of H_3BTC (0.021 g, 0.1 mmol) dissolved in 4 mL of methanol, with careful addition of imidazole (0.0345 g, 0.4 mmol). White block crystals with near quantitative yield were formed after ca. 1 day. The final products were washed thoroughly with fresh DI water, isolated by vacuum filtration, and dried at room temperature. A quantitative analysis of the crystals obtained was performed by CHN analysis. Anal. calcd (found) for $C_{18}H_8O_{17}Pb_2$: C, 23.74 (23.65); H, 0.89 (0.90).

Synthesis of Pb(HBTC)(DMF) (3). $Pb(NO_3)_2$ (0.0331 g, 0.1 mmol) dissolved in 4 mL of distilled water was carefully layered on top of H_3BTC (0.021 g, 0.1 mmol) dissolved in 2 mL of DMF. White plate-like crystals were formed in close to quantitative yield after ca. 1 day. The final products were either kept as they are in mother liquor or washed thoroughly with fresh DI water, isolated by vacuum filtration, and dried at room temperature. A quantitative analysis of the crystals was not performed due to decomposition of the product outside of the mother liquor.

X-ray Crystallography. X-ray intensity data from colorless crystals (**1**−**3**) were measured between 203(2) to 296(2) K using a Bruker SMART APEX diffractometer (Mo Kα radiation, λ = 0.71073 Å). Direct methods structure solution, difference Fourier calculations, and full-matrix least-squares refinement against F^2 were performed with SHELXTL.[67]

Powder X-ray Diffraction. Ground mixtures of polycrystalline powders and/or single crystals of the samples were used to collect powder X-ray diffraction patterns using a PanAlytical X'Pert Pro powder diffractometer (Cu Kα radiation λ = 1.5418 Å) over the 2θ range of 5−50°, with a step size of 0.02° and a scan speed of 0.25°/min. The measured patterns were compared to the simulated diffraction patterns using the respective single crystal data.

RESULTS AND DISCUSSION

Syntheses. Air-stable compounds **1** and **2** with nearly quantitative yield were identified by the reaction of aqueous-based $Pb(NO_3)_2$ with 1,4-dioxane and methanol solution of H_3BTC in the presence of aniline and imidazole for compounds **1** and **2**, respectively, under dissolution−crystallization with optimized condition. Compound **3**, on the other hand, was found to be relatively unstable at ambient conditions; fresh batch with the use of mother liquor is

DOI: 10.1021/acs.cgd.9b00759
Cryst. Growth Des. 2019, 19, 6274−6282

Table 2. Representative Bond Lengths (Å) and Bond Angles (deg) of Compound 1[a]

Pb(1)−O(2)	2.414(6)	O(3)#2−Pb(1)−O(3)	114.74(13)
Pb(1)−O(4)#1	2.580(6)	O(2)−Pb(1)−O(1)	51.26(18)
Pb(1)−O(3)#2	2.639(6)	O(4)#1−Pb(1)−O(1)	91.36(17)
Pb(1)−O(3)	2.644(5)	O(3)#2−Pb(1)−O(1)	79.49(17)
Pb(1)−O(1)	2.651(5)	O(3)−Pb(1)−O(1)	142.61(18)
Pb(1)−O(4)	2.674(5)	O(2)−Pb(1)−O(4)	84.02(19)
O(2)−Pb(1)−O(4)#1	78.03(19)	O(4)#1−Pb(1)−O(4)	112.93(15)
O(2)−Pb(1)−O(3)#2	89.8(2)	O(3)#2−Pb(1)−O(4)	66.89(17)
O(4)#1−Pb(1)−O(3)#2	167.73(18)	O(3)−Pb(1)−O(4)	48.72(17)
O(2)−Pb(1)−O(3)	92.82(19)	O(1)−Pb(1)−O(4)	123.89(17)

[a]Symmetry transformations used to generate equivalent atoms: (1) $-x + 1/2, y + 1/2, -z + 1/2$ (2) $-x + 1/2, y - 1/2, -z + 1/2$ (3) $x, -y + 1, z - 1/2$ (4) $x, -y + 1, z + 1/2$ (5) $-x, y, -z + 1/2$.

Table 3. Representative Bond Lengths (Å) and Bond Angles (deg) of Compound 2[a]

O(1)−Pb(1)	2.580(7)	O(1)−Pb(1)−O(2)	49.1(2)
O(2)−Pb(1)	2.713(7)	O(4)#3−Pb(1)−O(2)	121.6(2)
O(3)−Pb(1)#1	2.661(7)	O(7)−Pb(1)−O(2)	73.8(2)
O(4)−Pb(1)#1	2.628(7)	O(3)#3−Pb(1)−O(2)	149.4(2)
O(4)−Pb(1)#2	2.738(7)	O(1)−Pb(1)−O(4)#2	71.1(2)
O(1)−Pb(1)	2.580(7)	O(4)#3−Pb(1)−O(4)#2	73.7(2)
O(7)−Pb(1)	2.633(9)	O(7)−Pb(1)−O(4)#2	138.6(2)
Pb(1)#1−O(4)−Pb(1)#2	106.3(2)	O(3)#3−Pb(1)−O(4)#2	110.1(2)
O(1)−Pb(1)−O(4)#3	72.7(2)	O(2)−Pb(1)−O(4)#2	90.5(2)
O(1)−Pb(1)−O(7)	69.7(2)	O(4)#3−Pb(1)−O(3)#3	49.4(2)
O(4)#3−Pb(1)−O(7)	82.3(2)	O(7)−Pb(1)−O(3)#3	75.9(2)
O(1)−Pb(1)−O(3)#3	115.4(2)		

[a]Symmetry transformations used to generate equivalent atoms: (1) x, y, z-1 (2) $-x + 1, -y, -z$+1 (3) $x, y, z + 1$.

Table 4. Representative Bond Lengths (Å) and Bond Angles (deg) of Compound 3[a]

O(1)−Pb(1)	2.415(6)	O(1)−Pb(1)−O(4)#3	89.12(18)
O(3)−Pb(1)#1	2.535(5)	O(1)−Pb(1)−O(3)#4	72.55(18)
O(4)−Pb(1)#2	2.423(5)	O(4)#3−Pb(1)−O(3)#4	81.60(16)
O(7)−Pb(1)	2.720(5)	O(1)−Pb(1)−O(7)	71.02(18)
C(10)−N(1)	1.323(11)	O(4)#3−Pb(1)−O(7)	75.62(18)
C(11)−N(1)	1.462(11)	O(3)#4−Pb(1)−O(7)	136.89(17)
C(12)−N(1)	1.434(11)	C(10)−N(1)−C(12)	124.1(8)
C(9)−O(3)	1.264(9)	C(10)−N(1)−C(11)	118.0(8)

[a]Symmetry transformations used to generate equivalent atoms: (1) $-x + 1/2, y + 1/2, -z + 1/2$ (2) $x + 1, y, z$ (3) $x - 1, y, z$ (4) $-x + 1/2, y - 1/2, -z + 1/2$.

required for structural characterizations. The structure was determined by single-crystal X-ray diffraction, and its single phase purity was examined by bulk sample measurements using powder X-ray diffraction coupled with TGA and CHN analysis. Prior to this discovery, we attempted several synthetic conditions to obtain quantitative yields, which involved combinations of the following variables, such as (a) molar ratio of $Pb(NO_3)_2$ and H_3BTC, (b) variety of solvent or mixture of solvents. All three compounds were found to change their structures during storage, even in the presence of mother liquors.

The use of modulator, such as monoprotic acid or monocarboxylic acid, is often adopted to produce an air-stable transition metal (TM)-based MOFs with quantitative yield.[68−71] Further, Li et. al clarified that the use of an appropriate modulator, in some cases without being present in the structure, can modify the surface structure of TM-based MOFs, and thus it greatly enhances the stability and performance of the resulting MOF.[72] On the basis of our previous report, a borderline organic base is a suitable modulator for a borderline acid of Pb-based MOCP resulting in a stable and phase pure compound,[41] in accordance to Pearson's hard−soft acid base (HSAB) concept.[73,74] Adopting the above, we found that the use of aniline and imidazole, after several trials using other N-containing ligands, was required to make stable compounds of **1** and **2**, respectively. The unidentified peaks gradually disappeared as the suitable N-donor ligand was added during reaction that eventually, after optimizing the synthetic conditions, reached a phase pure with close to quantitative yields. At the moment, using the above-mentioned synthetic conditions for **1** and **2**, we could not detect the presence of aniline nor imidazole within the structures crystallographically nor by TGA nor CHN analysis, which supports the role of modulator for aniline and imidazole in these cases. Further investigations to examine the role of the modulator during synthesis, reaction mechanism, and resulting structural defect vs performance are currently ongoing.

Unfortunately, attempts to make an air-stable compound **3** were unsuccessful. Attempts to obtain these three phases by simple solvent exchange were unfruitful either. Activation

DOI: 10.1021/acs.cgd.9b00759
Cryst. Growth Des. 2019, 19, 6274−6282

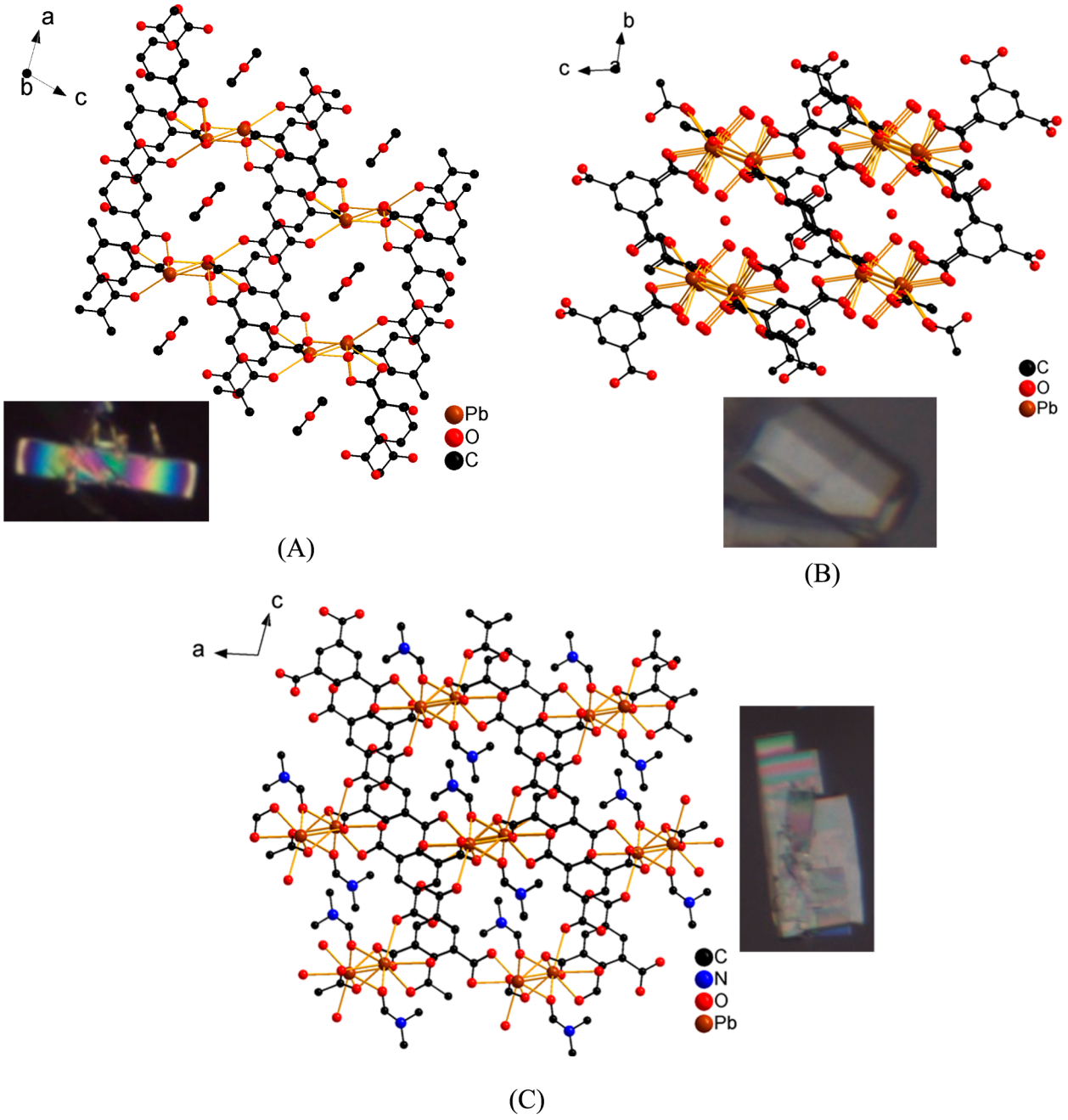

Figure 1. Three-dimensional MOF structures of (A) 1 viewed along the *b*-axis, (B) 2 viewed along the *a*-axis, (C) 3 viewed along the *b*-axis, with insets show the corresponding optical microscopy image of each crystal.

attempts for **1** and **2**, starting from rather harsh thermal activation to relatively milder supercritical CO_2 as well as solvent exchange activations, were unsuccessful.

Structural Description. The single-crystal structure refinements with their relevant crystallographic data for **1**−**3** are found in Table 1. Tables 2, 3, and 4 show representative bond distances and angles of compounds **1**−**3**, respectively. Figure S1A depicts the asymmetric unit of **1**, which consists of one lead atom site, one monoprotonated ligand ($HBTC^-$), and a half molecule of uncoordinated 1,4-dioxane. The oxygen atoms of the $HBTC^-$ ligand complete the coordination sphere around the lead cation, forming a distorted pentagonal bipyramid, PbO_7, Figure S1B. The asymmetric units of compounds **2** and **3**, also comprised of one lead cation, one monoprotonated BTC ($HBTC^-$) ligand, with additional five uncoordinated molecular waters for **2** and one coordinated DMF for **3**. A distorted bicapped pentagonal bipyramid, PbO_9, is observed for both **2** and **3** with coordinated oxygen atoms solely from $HBTC^-$ ligand for **2**, Figure S2 whereas **3** has an additional coordinated oxygen from DMF, Figure S3. Such a distorted polyhedral has also been observed in other lead-based coordination compounds.[75−80] The Pb−O bond length falls into the range of 2.415(6)−2.738(7) Å, typically observed in Pb-based coordination polymers.[75−80] All coordination modes of $HBTC^-$ ligand around the Pb center for **1**−**3** show *O,O*-chelation, oxygen bridging, monodentate, as well as uncoordinated oxygen atoms, which includes oxygen bridging from DMF in **3**, Figures S1−S3.

The three compounds are built from slightly different 1D structures, in which PbO_x (x = 7 for **1**, and 9 for **2** and **3**)

DOI: 10.1021/acs.cgd.9b00759
Cryst. Growth Des. 2019, 19, 6274−6282

polyhedra are linked by oxygen bridging in a zigzag manner to form 1D structures of $(Pb_2O_{12})_n$, $(Pb_2O_{16})_n$, and $(Pb_2O_{15})_n$ moieties for **1**–**3**, respectively, Figure S4. $(Pb_2O_{12})_n$ and $(Pb_2O_{15})_n$ moieties extend along the *b*-axis, whereas $(Pb_2O_{16})_n$ stretches along the *a*-direction. Double oxygen bridges with a zigzag pattern were observed for **1** (Figure S4) exhibiting a nearly straight O–Pb–O angle (167.8°), whereas **2** and **3** exhibit slightly bent zigzag patterns (O–Pb–O angle of 150.8° for **2** and 136.8° for **3**). Additional bridging oxygen (from DMF) is observed for **3**, Figure S4. Unlike the 1D moieties of **1** and **2** which comprise alternate polyhedral related by 2_1 screw axis, an inversion center relates the alternate polyhedral in **3** forming the 1D building block of the compound, Figure S4. Such distinct 1D building blocks, templated by a different solvent, determine their final 3D structures with slightly different frameworks and pore sizes to accommodate their corresponding solvent in their infinite 1D channel, Figure 1.

In compound **1**, the $HBTC^-$ ligands connect the 1D $(Pb_2O_{12})_n$ moieties in both *a*- and *c*-directions to form a porous 3D framework in which each 1D moiety is related by a glide plane along the *c*-directions, Figure 1. The $HBTC^-$ ligands also link the 1D $(Pb_2O_{16})_n$ in *b*- and *c*-directions forming a porous 3D framework of **2**, in which an *ac* mirror plane relates each $(Pb_2O_{16})_n$ moiety, Figure 1. As shown in Figure 1, the 1D $(Pb_2O_{15})_n$ moieties, related by a glide plane along the *c*-axis, are connected in *a*- and *c*-directions through $HBTC^-$ ligands to construct a 3D framework of **3**. Compounds **1** and **2** have a rather similar pore size (~7.50 Å) and are bigger than that of compound **3** (~3.05 Å pore size).

The topological analysis[81] of the three 3D structures reveals a 5-c uninodal net with a topological symbol of $\{4^6.6^4\}$ for both **1** and **2**, whereas a topological symbol of $\{4^6.5^2.6^2\}\{4^6.5^6.6^3\}$ simplified as a 5,6-c 2 nodal net is observed for compound **3**.

Another common feature of the three compounds that may contribute to structural rigidity is the monoprotonated dicarboxylic acid with Lewis base oxygen atoms (O(5) atoms of $HBTC^-$ ligand) located within the chains. There are weak hydrogen bonds, bond distances of 1.79 and 1.89 Å, between O(2) atoms of $HBTC^-$ ligand and H(5) atoms of the monoprotonated dicarboxylic acid as shown in dashed blue bonds for **2** and **3**, respectively, Figure S5. For compound **1**, the weak hydrogen bond with a bond length of 1.85 Å, forms between O(1) atoms of $HBTC^-$ ligand and H(5) atoms of the monoprotonated dicarboxylic acid. The presence of a Lewis base in these compounds is confirmed by attenuated total reflectance Fourier-transform infrared (ATR FTIR) spectra from the observation of a peak around 3575 cm^{-1}, indicating the existence of weakly hydrogen-bonded hydroxyl groups, Figure S6, confirming the observation in the crystal structure. Reduction of proton exchange due to relatively long hydrogen bonds leads to a relatively sharp O–H stretch. A sharper peak, for a comparison, would be observed at 3600 cm^{-1} for a fully free O–H group of carboxylic acid in MOCP.[82]

Powder X-ray diffraction was used to confirm the purity of all compounds as it can provide phase purity information and also reveal the presence or absence of polymorphs. PXRD patterns of the products obtained after optimized synthetic conditions are shown in Figure 2, showing a pure phase of **1** and **2** and that no additional polymorph is present in the sample used for further PL study. Washed and dried compound **3**, however, was found to coexist with an unknown impurity, Figure S7, even after several optimization attempts;

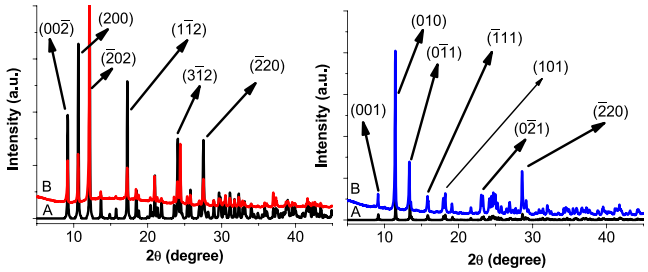

Figure 2. Powder X-ray diffraction patterns of (left) simulated, A, and observed, B, patterns of **1**; (right) simulated, A, and observed, B, patterns of **2**.

therefore, no further property is reported besides structural characterizations. The bulk phase purity of **1** and **2** is further confirmed by TGA analysis in which the observed weight losses of the corresponding solvent and the ligand are closely matched with the expected values calculated from formulas obtained from crystallographic refinements, Figure S8. This may also support that, within the synthetic conditions used in here, neither of the modulator is present in the structure, in conjunction with crystallographic refinement results as well as CHN analysis. The bulk crystal morphologies show the corresponding ribbon-like crystals for **1** and block-like crystals for **2** as shown in optical images, Figure 1, and SEM images, Figure 3.

Photoluminescence (PL). The use of luminescing ligand in luminescing MOF is advantageous in two ways: increasing PL intensity and/or shifting emission maxima for tunable PL color. The latter phenomena has been reported to relate to white emission reported in several MOFs.[64−66]

The room temperature, solid state emission spectra of the as-received H_3BTC ligand, and compounds **1** and **2**, including their digital images representing their PL colors, are shown in Figure 4. Compound **1**, when excited at 350 nm, emits a pale greenish yellow color with a broad peak covering 530–570 nm, Figure 4. Contrasting the UV–vis spectrum **1** to that of H_3BTC, both intraligand (ILCT) and ligand-to-metal charge transfers (LMCT) may be responsible for the observed emission spectrum. ILCT is corroborated by a similar absorption band that appears in both **1** and H_3BTC at a maximum of 302 nm. The disappearance of the broad absorption shoulder of the ligand in **1** at 330 nm validates the LMCT, Figure S9.

A bluish-white luminescence is observed for as-received H_3BTC with a broad emission spectrum covering almost the entire visible range (420–620 nm) with several maxima at 490, 544, and 615 nm when excited at 350 nm, Figure 4. Such emission is typically due to n → π^* and/or π → π^* transition.[64−66] A more pronounced "white" luminescent is emitted from compound **2** with a rather broad emission spectrum also at the 420–620 nm range, Figure 4. An additional feature of a shoulder band in the yellow range (560–580 nm) is clearly observed for **2** compared to that of ligand, which can be partly ascribed to metal-to-ligand charge transfer, MLCT.[64−66]

Overall, the observed near-white light emission of **2** could be attributed to LMCT and/or MLCT as well as ligand-centered transitions (ILCT), which correspond well to UV–vis spectra study, Figure S9. Compared to the spectrum of the as-received H_3BTC ligand, the disappearance of a broad shoulder at 330 nm in **2** may indicate the presence of LMCT, and the

DOI: 10.1021/acs.cgd.9b00759
Cryst. Growth Des. 2019, 19, 6274–6282

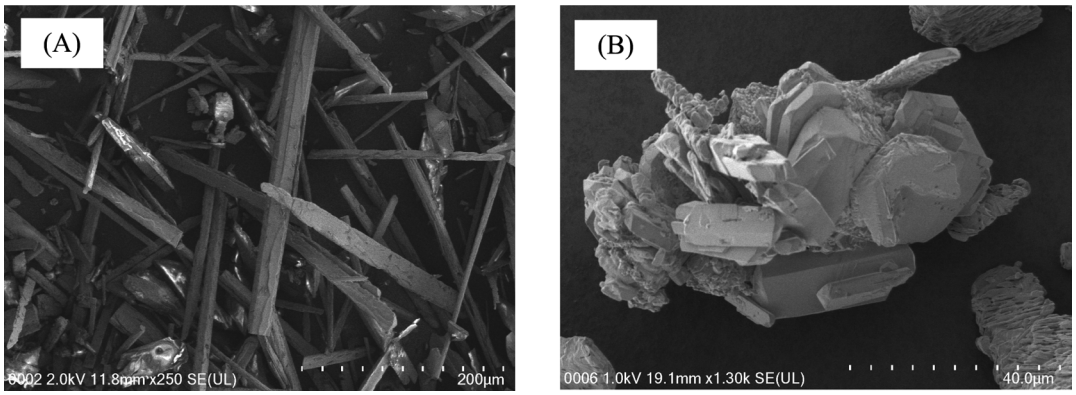

Figure 3. SEM images of (A) ribbon-like crystals of compound **1**, (B) block-like crystals of compound **2**.

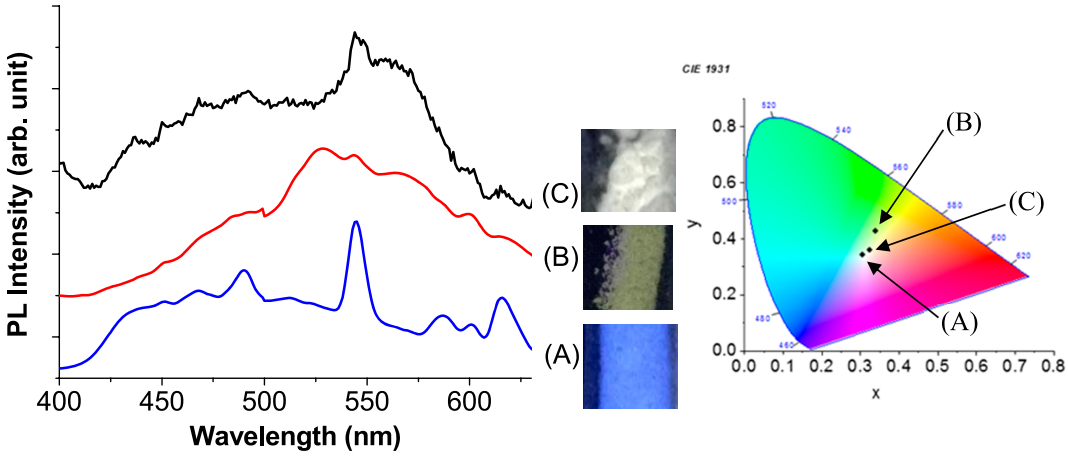

Figure 4. (Left) Solid-state emission spectra and the corresponding PL color images of (A) H_3BTC, (B) **1**, and (C) **2**; (right) corresponding CIE chromaticity diagram for H_3BTC (A), compounds **1** (B) and **2** (C).

emergence of new maxima at 228 nm in **2** signals the existence of MLCT. Further, a similar maxima at 302 nm indicates ILCT also occurring in **2**. All of these transitions are represented by a broad emission spectrum that leads to near-white PL color emitted from **2**. Such a broad, white emission spectrum is not only observed in Pb-based MOFs but also is reported in other Pb-based compounds, such as Pb-based perovskite halides, in which such a broad spectrum signature may stem from excition self-trapping.[62,63]

The quantified colors of the emissions of all compounds are plotted in the Commission Internationale l'Eclairage (CIE) chromaticity diagram, Figure 4. The as-received H_3BTC has CIE coordinates of (0.30, 0.34), giving a white with blue tinge gamut, in accordance to the observed PL image, when excited at 350 nm. Compound **2** exhibits a near-white color gamut, when excited at 350 nm, with CIE coordinates of (0.33, 0.36), showing the potential for a single-component white LED application. Several Pb-based MOFs were also reported as a near-white light single-component phosphor with CIE coordinates very close to ideal (0.33, 0.33). The white light emission in these papers were likely due to a combination of ILCT, LMCT, and/or MLCT as well.[64−66] As expected, compound **1** gives greenish yellow CIE coordinates of (0.34, 0.44) under 350 nm excitation.

CONCLUSION

In summary, we have synthesized three new lead frameworks based on the H_3BTC ligand using a simple dissolution−crystallization method. Utilizing the HSAB principle, further, we have successfully changed the unstable compounds of **1** and **2** to be their air-stable versions by adding an amount of aniline and imidazole, respectively, and therefore they can be used for further bulk applications. The two compounds show PL colors different from that of the H_3BTC ligand, indicating a successful charge transfer. Compound **1** was found to luminesce pale greenish yellow under 350 nm excitation, while an interesting near-white emission was observed for **2** when excited at 350 nm. The latter has a potential for a single-phase, white-light emitting compound for solid-state lighting applications.

ASSOCIATED CONTENT

Supporting Information

The Supporting Information is available free of charge on the ACS Publications website at DOI: 10.1021/acs.cgd.9b00759.

Figures S1−S9 (PDF)

Accession Codes

CCDC 1823911−1823913 contain the supplementary crystallographic data for this paper. These data can be obtained free of charge via www.ccdc.cam.ac.uk/data_request/cif, or by emailing data_request@ccdc.cam.ac.uk, or by contacting The Cambridge Crystallographic Data Centre, 12 Union Road, Cambridge CB2 1EZ, UK; fax: +44 1223 336033.

DOI: 10.1021/acs.cgd.9b00759
Cryst. Growth Des. 2019, 19, 6274−6282

AUTHOR INFORMATION

Corresponding Author

*E-mail: wibowor@gmail.com.

ORCID

Hongil Jo: 0000-0002-0627-4921
Kang Min Ok: 0000-0002-7195-9089
Arief C. Wibowo: 0000-0002-2454-4307

Notes

The authors declare no competing financial interest.

ACKNOWLEDGMENTS

Financial support for this research was provided by HIR Chancellory Grant UM.C/625/1/HIR/211 from the University of Malaya and FRGS, Ministry of Education, Malaysia, Project No. FP 037-2014A. K.M.O. acknowledges the financial support from the National Research Foundation of Korea funded by the Ministry of Science and ICT (Grant Nos. 2018R1A5A1025208 and 2019R1A2C3005530).

REFERENCES

(1) Furukawa, H.; Cordova, K. E.; O'Keeffe, M.; Yaghi, O. M. The Chemistry and Applications of Metal-Organic Frameworks. *Science* **2013**, *341*, 974−988.

(2) Kuppler, R. J.; Timmons, D. J.; Fang, Q.-R.; Li, J.-R.; Makal, T. A.; Young, M. D.; Yuan, D.; Zhao, D.; Zhuang, W.; Zhou, H.-C. Potential applications of metal-organic frameworks. *Coord. Chem. Rev.* **2009**, *253*, 3042−3066.

(3) Burtch, N. C.; Jasuja, H.; Walton, K. S. Water Stability and Adsorption in Metal-Organic Frameworks. *Chem. Rev.* **2014**, *114*, 10575−10612.

(4) Ferey, G.; Serre, C.; Devic, T.; Maurin, G.; Jobic, H.; Llewellyn, P. L.; De Weireld, G.; Vimont, A.; Daturi, M.; Chang, J.-S. Why hybrid porous solid capture greenhouse gases? *Chem. Soc. Rev.* **2011**, *40*, 550−562.

(5) Barea, E.; Montoro, C.; Navarro, J. A. R. Toxic gas removal by MOF. *Chem. Soc. Rev.* **2014**, *43*, 5419−5430.

(6) Wang, X.-Y.; Avendano, C.; Dunbar, K. R. Magnetic MOF based on 4d and 5d TM. *Chem. Soc. Rev.* **2011**, *40*, 3213−3238.

(7) Weng, D.-F.; Wang, Z.-M.; Gao, S. Framework-structured weak ferromagnets. *Chem. Soc. Rev.* **2011**, *40*, 3157−3181.

(8) Cui, Y.; Yue, Y.; Qian, G.; Chen, B. Luminescent Functional MOF. *Chem. Rev.* **2012**, *112*, 1126−1162.

(9) Heine, J.; Muller-Buschbaum, K. Engineering Luminescence in MOF. *Chem. Soc. Rev.* **2013**, *42*, 9232−9242.

(10) Rocha, J.; Carlos, L. D.; Almeida Paz, F. A.; Ananias, D. Ln Based Luminescent MOF. *Chem. Soc. Rev.* **2011**, *40*, 926−940.

(11) Akhbari, K.; Morsali, A. Solid- and solution-state structural transformations in flexible lead(II) supramolecular polymers. *CrystEngComm* **2013**, *15*, 8915−8918.

(12) Burrows, A. D.; Mahon, M. F.; Sebestyen, V. M.; Lan, Y.; Powell, A. K. Synthesis, Structures, And Magnetic Behavior of New Anionic Copper(II) Sulfate Aggregates and Chains. *Inorg. Chem.* **2012**, *51*, 10983−10989.

(13) Chakrabarti, S.; Natarajan, S. A reactive intermediate in the synthesis of iron arsenates: Synthesis of the first one-dimensional iron arsenate oxalate and its transformation into two- and three-dimensional iron arsenates. *Angew. Chem., Int. Ed.* **2002**, *41*, 1224−1226.

(14) Dan, M.; Udayakumar, D.; Rao, C. N. R. Transformation of a 4-membered ring zinc phosphate SBU to a sodalite-related 3-dimensional structure through a linear chain structure. *Chem. Commun.* **2003**, 2212−2213.

(15) Fu, J.; Fu, J.; Mu, Y.; Liu, Y.; Hou, H.; Fan, Y. The structural transformation from 2D layers to 3D nets by solvent-mediated cation-exchange reaction. *Inorg. Chem. Commun.* **2011**, *14*, 1823−1826.

(16) Guo, Y.-P.; Li, D.-Y.; Li, G.-T. Poly bis{mu(2)-N-2,N-6-bis (pyridin-3-yl)methyl pyridine-2,6-dicarboxam ide}-dichloridonickel-(II) N,N-dimethylformamide tetrasolvate. *Acta Crystallogr., Sect. C: Cryst. Struct. Commun.* **2012**, *68*, M284−m286.

(17) Huang, C.; Wang, Y.; Wei, C.; Li, N.; Ji, F.; Wu, J.; Hou, H. Cation-exchange-induced single-crystal-to-single-crystal transformations of a nanoporous coordination complex. *Inorg. Chem. Commun.* **2013**, *32*, 68−73.

(18) Jeon, Y.; Cheon, S.; Cho, S.; Lee, K. Y.; Kim, T. H.; Kim, J. Controlled Reversible Crystal Transformation of Cu(I) Supramolecular Isomers. *Cryst. Growth Des.* **2014**, *14*, 2105−2109.

(19) Kang, M.; Yang, G.-P.; Hou, L.; Wu, W.-P.; Wu, Y.-L.; Wang, Y.-Y. Peculiar phenomena of structural transformations triggered from a nickel coordination polymer. *CrystEngComm* **2015**, *17*, 1839−1847.

(20) Li, X.; Gong, Y.; Zhao, H.; Wang, R. Solvent-mediated crystal-to-crystal transformations from a cationic homometallic metal-organic framework to heterometallic frameworks. *CrystEngComm* **2014**, *16*, 8818−8824.

(21) Li, Y.-M.; Yu, Y.-H.; Peng, Y.-H.; Wu, B.-L.; Zhang, H.-Y. A tetragonal molecular cage and polymeric macrocyclic complex based on a clip-like bis-pyridyl-bis-amide ligand. *J. Coord. Chem.* **2012**, *65*, 2771−2956.

(22) Liang, P. C.; Liu, H. K.; Yeh, C. T.; Lin, C. H.; Zima, V. Supramolecular Assembly of Calcium Metal-Organic Frameworks with Structural Transformations. *Cryst. Growth Des.* **2011**, *11*, 699−708.

(23) Loganathan, N.; Roodt, A. Crystal structure of mu-oxo-di-mu-sulfato-kappa O-2:O′-bis (2,2′-bipyridine-kappa N-2,N′)-bis-(dimethylsulfoxide-kappa O)-diiron(III) monohydrate, $C_{24}H_{30}Fe_2N_4O_{12}S_4$. *Z. Kristallogr. - New Cryst. Struct.* **2013**, *228*, 476−478.

(24) Lu, H.; Mu, Y.; Li, J.; Wu, D.; Hou, H.; Fan, Y. Coordinated anion exchange induced structural transformation from a trinuclear cage to a 3D interpenetrated framework with the solvent-mediated mechanism. *Inorg. Chim. Acta* **2012**, *387*, 450−454.

(25) Mahata, P.; Mellot-Draznieks, C.; Roy, P.; Natarajan, S. Solid State and Solution Mediated Multistep Sequential Transformations in Metal-Organic Coordination Networks. *Cryst. Growth Des.* **2013**, *13*, 155−168.

(26) Murugavel, R.; Walawalkar, M. G.; Dan, M.; Roesky, H. W.; Rao, C. N. R. Transformations of molecules and secondary building units to materials: A bottom-up approach. *Acc. Chem. Res.* **2004**, *37*, 763−774.

(27) Natarajan, S. Synthesis of a layered zinc phosphate, NH3-(CH2)(2)NH2(CH2)(3)NH3 Zn-2(PO4)(HPO4)2 center dot H2O, and its transformation to a extra-large pore three-dimensional zinc phosphate, NH3(CH2)(2)NH2(CH2)(3)NH3 Zn-3(PO4)-(HPO4)(3). *Chem. Commun.* **2002**, *13*, 780−781.

(28) Norquist, A. J.; O'Hare, D. Kinetic and mechanistic investigations of hydrothermal transformations in zinc phosphates. *J. Am. Chem. Soc.* **2004**, *126*, 6673−6679.

(29) Peedikakkal, A. M. P.; Vittal, J. J. Structural Transformations of Pb(II)-trans-1,2-bis(4 '-pyridyl)ethene Coordination Polymers in Solution. *Cryst. Growth Des.* **2011**, *11*, 4697−4703.

(30) Shimoni-Livny, L.; Glusker, J. P.; Bock, C. W. *Inorg. Chem.* **1998**, *37*, 1853−1867.

(31) Thirumurugan, A.; Rao, C. N. R. 1,2-, 1,3- and 1,4-benzenedicarboxylates of Cd and Zn of different dimensionalities: Process of formation of the three-dimensional structure. *J. Mater. Chem.* **2005**, *15*, 3852−3858.

(32) Tripathy, D.; Pal, A. K.; Hanan, G. S.; Chand, D. K. Palladium(II) driven self-assembly of a saturated quadruple-stranded metallo helicate. *Dalton Trans* **2012**, *41*, 11273−11275.

(33) Wang, X.; Huang, J.; Liu, L.; Liu, G.; Lin, H.; Zhang, J.; Chen, N.; Qu, Y. Assembly of Zn/Cd coordination polymers containing helixes or polycatenane structures tuned by the tri-pyridyl-bis-amide ligands with different spacer: syntheses, structures, photoluminescent and photocatalytic properties. *CrystEngComm* **2013**, *15*, 1960−1969.

DOI: 10.1021/acs.cgd.9b00759
Cryst. Growth Des. 2019, 19, 6274−6282

(34) Wang, X.-L.; Chen, N.-L.; Liu, G.-C.; Lin, H.-Y.; Zhang, J.-W. Six tubular/helical nickel(II) coordination polymers tuned by V-like tri-pyridyl-bis-amide and dicarboxylates with different spacers. *Inorg. Chim. Acta* **2014**, *421*, 473−480.
(35) Wang, X.-L.; Zhao, W.; Hou, J.-L.; Zhang, J.-W.; Lu, Q.-L.; Luan, J.; Liu, G.-C. Zero-, one- and two-dimensional bis-triazole-bis-amide-based copper(II) complexes tuned by polycarboxylates with different protonation degrees: assembly, structures and properties. *Transition Met. Chem.* **2013**, *38*, 827−833.
(36) Wiebcke, M.; Kuhn, C.; Wildermuth, G. Hydrothermal reversible interconversion of two zincophosphates with three-dimensional open frameworks containing diprotonated 1,4-diazacycloheptane molecules. *J. Solid State Chem.* **2005**, *178*, 694.
(37) Xu, C.; Wang, X.; Ding, D.; Hou, H.; Fan, Y. Tunable structures aroused by cation exchange reaction of solvent-mediated mechanism. *Inorg. Chem. Commun.* **2011**, *14*, 1410−1424.
(38) Xu, H.-H.; Tao, X.; Li, Y.-Q.; Shen, Y.-Z.; Wei, Y.-H. Bis mu-N,N ′-bis(quinolin-8-yl)pyridine-2,6-dicarboxamido dizinc(II) dichloromethane disolvate. *Acta Crystallogr., Sect. C: Cryst. Struct. Commun.* **2011**, *67*, M93−m95.
(39) Zhang, T.-Z.; Zhang, Z.-M.; Lu, Y.; Fu, H.; Wang, E.-B. Expansion of sodalite-type metal-organic frameworks with heterometallic metal-oxo cluster and its cation exchange property. *CrystEngComm* **2013**, *15*, 459−462.
(40) Zhou, X. P.; Xu, Z. T.; Zeller, M.; Hunter, A. D.; Chui, S. S. Y.; Che, C. M. Semirigid Aromatic Sulfone-Carboxylate Molecule for Dynamic Coordination Networks: Multiple Substitutions of the Ancillary Ligands. *Inorg. Chem.* **2011**, *50*, 7142−7149.
(41) Wardana, F. Y.; Ng, S.-W.; Wibowo, A. C. The Lead Coordination Polymers Containing Pyrazine-2,3-Dicarboxylic Acid: Rapid Structural Transformations and Cation Exchange. *Cryst. Growth Des.* **2015**, *15*, 5930−5938.
(42) Brozek, C. K.; Dinca, M. Cation exchange at the secondary building units of metal-organic frameworks. *Chem. Soc. Rev.*, **2014***43*, 5456−5467.
(43) Hamisu, A. M.; Wardana, F. Y.; Ariffin, A.; Baig, I.; Malliakas, C. D.; Wibowo, A. C. A new synthetic approach for substitutional solid solutions in a 3D coordination polymer: Cation vacancy, and tunable photoluminescence. *J. Solid State Chem.* **2019**, *279*, 120948.
(44) Chui, S. S.; Lo, S. M.; Charmant, J. P.; Orpen, A. G.; Williams, I. D. A Chemically Functionalizable Nanoporous Material [Cu3(TMA)2(H2O)3]n. *Science* **1999**, *283*, 1148−1150.
(45) Esswein, A. J.; Nocera, D. G. Hydrogen production by molecular photocatalysis. *Chem. Rev.* **2007**, *107*, 4022−4047.
(46) Liang, K.; Ricco, R.; Doherty, C. M.; Styles, M. J.; Bell, S.; Kirby, N.; Mudie, S.; Haylock, D.; Hill, A. J.; Doonan, C. J.; Falcaro, P. Biomimetic mineralization of metal-organic frameworks as protective coatings for biomacromolecules. *Nat. Commun.* **2015**, *6*, 7240.
(47) Talin, A. A.; Centrone, A.; Ford, A. C.; Foster, M. E.; Stavila, V.; Haney, P.; Kinney, R. A.; Szalai, V.; El Gabaly, F.; Yoon, H. P.; Léonard, F.; Allendorf, M. D. Tunable electrical conductivity in metal-organic framework thin-film devices. *Science* **2014**, *343*, 66−69.
(48) Tan, Y. C.; Zeng, H. C. Lewis basicity generated by localised charge imbalance in noble metal nanoparticle-embedded defective metal-organic frameworks. *Nat. Commun.* **2018**, *9*, 4326.
(49) Briand, G. G.; Burford, N.: Coordination complexes of bismuth(III) involving organic ligands with pnictogen or chalcogen donors. In *Adv. Inorg. Chem.*; Academic Press, 2000; Vol. *50*; pp 285−357.
(50) Fan, S. R.; Zhu, L. G. Syntheses, structures, and characterizations of four new lead(II) 5-sulfosalicylate complexes with both chelating and bridging neutral ligands. *Inorg. Chem.* **2007**, *46*, 6785−6793.
(51) Pearson, R. G. Hard and Soft Acids and Bases. *J. Am. Chem. Soc.* **1963**, *85*, 3533−3539.
(52) Rao, K. P.; Thirumurugan, A.; Rao, C. N. Lamellar and three-dimensional hybrid compounds formed by cyclohexene- and cyclohexanedicarboxylates of Pb, La, and Cd. *Chem. - Eur. J.* **2007**, *13*, 3193−3201.
(53) Thirumurugan, A.; Sanguramath, R. A.; Rao, C. N. Hybrid structures formed by lead 1,3-cyclohexanedicarboxylates. *Inorg. Chem.* **2008**, *47*, 823−831.
(54) Yang, J.; Ma, J. F.; Liu, Y. Y.; Ma, J. C.; Batten, S. R. Organic-acid effect on the structures of a series of lead(II) complexes. *Inorg. Chem.* **2007**, *46*, 6542−6555.
(55) Yang, J.; Ma, J.-F.; Liu, Y.-Y.; Ma, J.-C.; Batten, S. R. A Series of Lead(II) Complexes with π-π Stackings: Structural Diversities by Varying the Ligands. *Cryst. Growth Des.* **2009**, *9*, 1894−1911.
(56) Zhao, Y. H.; Xu, H. B.; Fu, Y. M.; Shao, K. Z.; Yang, S. Y.; Su, Z. M.; Hao, X. R.; Zhu, D. X.; Wang, E. B. A Series of Lead(II)-Organic Frameworks Based on Pyridyl Carboxylate Acid N-Oxide Derivatives: Syntheses, Structures, and Luminescent Properties. *Cryst. Growth Des.* **2008**, *8*, 3566−3576.
(57) Chen, J.; Wang, X.-C.; Li, C.-X. *Acta Crystallogr., Sect. E: Struct. Rep. Online* **2010**, *66*, m1651−m1652.
(58) Sel, K.; Demirci, S.; Ozturk, O. F.; Aktas, N.; Sahiner, N. NH3 gas sensing applications of MOFs. *Microelectron. Eng.* **2015**, *136*, 71−76.
(59) Song, J.-L.; Mao, J.-G.; Sun, Y.-Q.; Clearfield, A. Novel Hybrid Porous 3D Networks of Lead(II) Diphosphonate and Triphosphonate Containing 1,3,5 Benzenetricarboxylate. *Eur. J. Inorg. Chem.* **2003**, *2003*, 4218−4226.
(60) Che, G.-B.; Chen, J.; Wang, X.-C.; Liu, C.-B.; Wang, C.-J.; Wang, S.-T.; Yan, Y.-S. A novel pillared double-layered Pb(II) coordination polymer based on 1,3,5-benzenetricarboxylic acid and dipyrido[3,2-a:2′,3′-c]-phenazine-2-carboxylic acid. *Inorg. Chem. Commun.* **2011**, *14*, 1086−1088.
(61) Xu, B.; Cai, Y.; Li, L.; Zhang, Z.; Li, C. Two novel Pb(II)-based heterometallic coordination polymers assembled from 1,3,5-benzenetricarboxylic acid: Syntheses, structures and luminescent properties. *J. Mol. Struct.* **2014**, *1059*, 320−324.
(62) Smith, M. D.; Connor, B. A.; Karunadasa, H. I. Tuning the Luminescence of Layered Halide Perovskites. *Chem. Rev.* **2019**, *119*, 3104−3139.
(63) Smith, M. D.; Karunadasa, H. I. White-Light Emission from Layered Halide Perovskites. *Acc. Chem. Res.* **2018**, *51*, 619−627.
(64) Peedikakkal, A. M. P.; Quah, H. S.; Chia, S.; Jalilov, A. S.; Shaikh, A. R.; Al-Mohsin, H. A.; Yadava, K.; Ji, W.; Vittal, J. J. Near-White Light Emission from Lead(II) Metal-Organic Frameworks. *Inorg. Chem.* **2018**, *57*, 11341−11348.
(65) Qi, H.-X.; Jo, H.; Ok, K. M. Pb[NC5H3(CO2)2]: a white light emitting single component coordination polymer revealing high quantum efficiency and thermal stability. *Inorg. Chem. Front.* **2018**, *5*, 1273−1276.
(66) Wibowo, A. C.; Vaughn, S. A.; Smith, M. D.; zur Loye, H.-C. *Inorg. Chem.* **2010**, *49*, 11001−11008.
(67) Sheldrick, G. M. *SHELXTL Ver. 6.*, 14 ed.; Bruker Analytical X-ray Systems, Inc.: Madison, WI, 2003.
(68) Hu, Z.; Castano, I.; Wang, S.; Wang, Y.; Peng, Y.; Qian, Y.; Chi, C.; Wang, X.; Zhao, D. Modulator Effects on the Water-Based Synthesis of Zr/Hf Metal-Organic Frameworks: Quantitative Relationship Studies between Modulator, Synthetic Condition, and Performance. *Cryst. Growth Des.* **2016**, *16*, 2295−2301.
(69) Vermoortele, F.; Bueken, B.; Le Bars, G.; Van de Voorde, B.; Vandichel, M.; Houthoofd, K.; Vimont, A.; Daturi, M.; Waroquier, M.; Van Speybroeck, V.; Kirschhock, C.; De Vos, D. E. Synthesis Modulation as a Tool To Increase the Catalytic Activity of Metal-Organic Frameworks: The Unique Case of UiO-66(Zr). *J. Am. Chem. Soc.* **2013**, *135*, 11465−11468.
(70) Webber, T. E.; Liu, W.-G.; Desai, S. P.; Lu, C. C.; Truhlar, D. G.; Penn, R. L. Role of a Modulator in the Synthesis of Phase-Pure NU-1000. *ACS Appl. Mater. Interfaces* **2017**, *9*, 39342−39346.
(71) Zahn, G.; Zerner, P.; Lippke, J.; Kempf, F. L.; Lilienthal, S.; Schroder, C. A.; Schneider, A. M.; Behrens, P. Insight into the mechanism of modulated syntheses: in situ synchrotron diffraction

DOI: 10.1021/acs.cgd.9b00759
Cryst. Growth Des. 2019, 19, 6274−6282

studies on the formation of Zr-fumarate MOF. *CrystEngComm* **2014**, *16*, 9198−9207.
(72) Li, X.; Wang, J.; Liu, X.; Liu, L.; Cha, D.; Zheng, X.; Yousef, A. A.; Song, K.; Zhu, Y.; Zhang, D.; Han, Y. Direct Imaging of Tunable Crystal Surface Structures of MOF MIL-101 Using High-Resolution Electron Microscopy. *J. Am. Chem. Soc.* **2019**, *141*12021.
(73) *Adv. Inorg. Chem.*; Briand, G. G.; Burford, N., Eds.; Academic Press, 2000; Vol. *50*.
(74) Pearson, R. G. *J. Am. Chem. Soc.* **1963**, *85*, 3533−3539.
(75) Davidovich, R. L.; Stavila, V.; Marinin, D. V.; Voit, E. I.; Whitmire, K. H. Stereochemistry of lead(II) complexes with oxygen donor ligands. *Coord. Chem. Rev.* **2009**, *253*, 1316−1352.
(76) Li, Q.-Y.; Yang, G.-W.; Ma, Y.-S.; Li, M.-J.; Zhou, Y. Synthesis and structural characterization of two novel 2D coordination polymers PbCl(atza) (n) and PbCl(a4-ptz) (n). *Inorg. Chem. Commun.* **2008**, *11*, 795−798.
(77) Wang, X.-W.; Han, L.; Cai, T.-J.; Zheng, Y.-Q.; Chen, J.-Z.; Deng, Q. A novel chiral doubly folded interpenetrating 3D metal-organic framework based on the flexible zwitterionic ligand. *Cryst. Growth Des.* **2007**, *7*, 1027−1030.
(78) Yu, X.-Y.; Xin, R.; Gao, W.-P.; Wang, N.; Zhang, X.; Yang, Y.-Y.; Qu, X.-S. Three Pb-II coordination polymers based on 2-(pyridin-2-yl)-1. H-imidazole-4,5-dicarboxylic acid: Syntheses, crystal structures, and fluorescent properties. *J. Solid State Chem.* **2013**, *204*, 314−320.
(79) Zhang, K.-L.; Pan, Z.-C.; Chang, Y.; Liu, W.-L.; Ng, S. W. Synthesis and characterization of an energetic three-dimensional metal-organic framework with blue photoluminescence. *Mater. Lett.* **2009**, *63*, 2136−2138.
(80) Zhao, J.; Li, L.; Wang, C.; Li, W.; Wang, R.; Zheng, X.; Hou, H. Unusual 3D pillared-layer Pb(II) complex supported by mercapto-triazole ligand: Synthesis, structure and luminescent property. *Inorg. Chem. Commun.* **2012**, *20*, 205−208.
(81) Blatov, V. A. Multipurpose crystallochemical analysis with the program package TOPOS. *IUCr CompComm Newsl.* **2006**, *7*, 4−38.
(82) Karagiaridi, O.; Vermeulen, N.; Klet, R. C.; Wang, T. C.; Moghadam, P. Z.; Al-Juaid, S. S.; Stoddart, J. F.; Hupp, J. T.; Farha, O. K. *Inorg. Chem.* **2015**, *54*, 1785−1790.

DOI: 10.1021/acs.cgd.9b00759
Cryst. Growth Des. 2019, 19, 6274−6282